第36卷第11期 2020年11月
无 机 化 学 学 报
CHINESE JOURNAL OF INORGANIC CHEMISTRY
Vol.36 No.11 2145-2156

焙烧温度对“软-硬”模板法制备的 $Pd/Ce_{0.65}Zr_{0.35}O_2$ 三效催化性能的影响

黄利华[1] 陈耀强*[,2]
([1]西南科技大学环境与资源学院,绵阳 621010)
([2]四川大学化学学院,成都 610064)

摘要: 采用“软-硬”模板法制备了具有高热稳定性的 $Ce_{0.65}Zr_{0.35}O_2$(CeZr)。考察了制备过程中焙烧温度对 $Ce_{0.65}Zr_{0.35}O_2$ 及其负载的单Pd三效催化剂(TWC)性能的影响。对样品进行了X射线衍射、比表面、拉曼光谱、X射线光电子能谱、储氧性能和 H_2 程序升温还原性能测试。结果表明:焙烧温度显著影响催化剂的结构和性能。随着焙烧温度的增加,$Ce_{0.65}Zr_{0.35}O_2$ 的比表面下降,但在1 000 ℃焙烧的样品比表面为61 $m^2\cdot g^{-1}$,显著高于同温度下直接在空气中焙烧的样品。由于高温导致了物相重组,$Ce_{0.65}Zr_{0.35}O_2$ 的储氧量和还原性能随着焙烧温度的增加而提升。由于高温烧结导致Pd分散性的下降,其负载的催化剂的还原性能随着焙烧温度的增加而下降,从而最终导致催化剂活性的降低。但在“软-硬”模板法中1 000 ℃焙烧的样品负载的催化剂依然显示出很好的三效催化性能,该催化剂上 C_3H_8、CO和NO的起燃温度分别为274、175和133 ℃,显著低于同温度下空气中直接焙烧的样品负载的催化剂。催化剂的氧化还原性能和Pd的分散性是影响催化活性的主要因素。

关键词: $Ce_{0.65}Zr_{0.35}O_2$; 高热稳定性; 催化性能
中图分类号: O643.36 文献标识码: A **文章编号:** 1001-4861(2020)11-2145-12
DOI: 10.11862/CJIC.2020.227

Effect of Calcination Temperature on Three-Way Catalytic Performance of $Pd/Ce_{0.65}Zr_{0.35}O_2$ Prepared by Soft-Hard Template Method

HUANG Li-Hua[1] CHEN Yao-Qiang*[,2]
([1]*Institute of Environment and Resources, Southwest University of Science and Technology, Mianyang, Sichuan* 621010, *China*)
([2]*College of Chemistry, Sichuan University, Chengdu* 610064, *China*)

Abstract: High thermal stability $Ce_{0.65}Zr_{0.35}O_2$(CeZr) was prepared by soft-hard template method. The influence of calcination temperature on properties of $Ce_{0.65}Zr_{0.35}O_2$ and its corresponding Pd based three-way catalyst (TWC) was investigated. The samples were analyzed by X-ray diffraction, surface area analysis, Raman spectrum, X-ray photoelectron spectroscopy, oxygen storage capacity and H_2-temperature-programmed reduction. The results indicate that the structure and redox properties are strongly influenced by calcination temperature. The structure properties, for instance, BET (Brunaner-Emmett-Teller) surface area declined along with the rise of temperature, but the BET surface area of the sample calcinated at 1 000 ℃ was 61 $m^2\cdot g^{-1}$, which was significantly higher than that calcinated direct in air at the same temperature. The OSC and reduction property of $Ce_{0.65}Zr_{0.35}O_2$ increased with the rise of calcination temperature because of phase rearrangement at high temperature. The redox property of their corresponding catalysts decreased due to descending of Pd dispersion, which results in decline of three-way catalytic activity at last. Although high temperature sintering led to decrease of catalytic performance, the catalyst prepared by soft-hard template method calcinated at 1 000 ℃ still had excellent activity. The light-off temperature for C_3H_8, CO and NO

收稿日期:2020-03-23。收修改稿日期:2020-06-22。
四川省教育厅(No.17ZB0457)资助项目。
*通信联系人。E-mail:nic7501@scu.edu.cn

was 274, 175 and 133 ℃, respectively, which was significantly lower than catalyst calcined direct in air at the same temperature. Redox property and dispersity of Pd are significant factors affecting activity of catalyst.

Keywords: $Ce_{0.65}Zr_{0.35}O_2$; high thermal stability; catalytic performance

0 Introduction

CeO_2-ZrO_2 is a key material used in automotive three-way catalysts (TWCs) on account of its outstanding oxygen storage capacity. Thermal stability of CeO_2-ZrO_2 at temperature up to 1 000 ℃ is an essential requirement taking into account its actual working conditions[1]. With the improvement of emission standards, there is an increasing demand for the thermal stability of CeO_2-ZrO_2 solid solutions at high temperature. This pushes researchers to develop new synthesis route. Several ways such as co-precipitation[2], microemulsion, hydrothermal and sol-gel method[3] have been applied to prepare these materials. Among these methods, co-precipitation is commonly used because of its inexpensive and flexible. In co-precipitation method, structure and property of the final product can be changed either by altering preparation conditions or introducing co-precipitation agents such as surfactants[4-6]. As surfactants can significantly enhance the surface area of CeO_2-ZrO_2, it has received widespread attention. But when the material is heat-treated to a high enough temperature (especially exceed 800 ℃), the mesoporous structure collapse and then cause significant decrease of specific surface and reducibility. To prevent sintering at high calcination temperature, Li′s[7] group reported a soft and hard process in the preparation of high thermal stability metal oxide (TiO_2, Nb_2O). In this method, amphiphilic di-block copolymer and metal salt solutions were first mixed to form sol. Then the sol was evaporated and subsequently calcinated in N_2. In this process, it decomposed into mixture of carbon and metal oxides in the inert gas. Serious sintering of metal oxide could be avoided due to encapsulating or isolating of carbon formed in calcination. The high specific surface area of nano-sized particles may be generated by subsequent low temperature air calcination to remove carbon species[7]. By using this method, CeO_2-ZrO_2 mixed oxides such as $Ce_{0.8}Zr_{0.2}O$[8], $Ce_{0.5}Zr_{0.5}O_2$[9] were also synthesized by other researchers. But these researches focused on their texture property such as BET (Brunaner-Emmett-Teller) surface area. The redox property and catalytic performance which are necessary and vital for automobile exhaust purification catalysts were almost not studied. Our previous studies[10] have disclosed that $Ce_{0.65}Zr_{0.35}O_2$ prepared by soft-hard template method behaved excellent catalytic performance. In this study, we focus on the impact of calcination temperature on structure, texture, oxygen storage capacity (OSC), redox properties of $Ce_{0.65}Zr_{0.35}O_2$. The performance of corresponding Pd-only catalysts was also intensively studied.

1 Experimental

1.1 Synthesis of $Ce_{0.65}Zr_{0.35}O_2$

$Ce_{0.65}Zr_{0.35}O_2$ was prepared according to the reference[10]. $Ce(NO_3)_3 \cdot 6H_2O$ was dissolved in deionized water, then $Zr(NO)_3$ was added into $Ce(NO_3)_3$ solution to form mixed solution. Copolymer solution (polyvinyl alcohol and polyethylene glycol) was added in the mixed solution. After being stirred for 1 h, ammonium carbonate solution was added in the mixed solution to form precipitate. The pH value of precipitation process was controlled at 9.0. The obtained precipitate was aged, filtered, washed, and then dried. The dried precipitate was calcined in atmosphere of N_2 at 500, 600, 700, 800, 1 000 ℃ for 6 h, respectively. In the process of calcination, the precipitate was decomposed and formed mixture of Ce-Zr oxides and carbon. In order to remove the carbon powder and obtain the final product, the carbonated product was calcinated in air at 450 ℃ for 3 h. The resultant sample was labelled as CeZr-Nx (x=5, 6, 7, 8, 10). For instance, CeZr-N5 was the sample calcined in N_2 at the temperature of 500 ℃. As a contrast, the sample calcinated direct in air at 1 000 ℃ was also prepared and named CeZr-A10.

1.2 Preparation of the catalysts

$Pd(NO_3)_2$ solution was impregnated onto

$Ce_{0.65}Zr_{0.35}O_2$ materials to form catalysts. The catalysts were first wet milled to form uniform slurry and then smeared onto ceramic honeycomb to form monolithic catalysts. By drying and roasting (550 ℃ for 3 h), the final catalysts were obtained. The content of PdO was 2%(*w*/*w*). The final catalysts were labelled as Pd/CeZr-N*x*, which corresponded to the supports calcined at different temperatures.

1.3 Characterization

D/Max-rA diffraction instrument was used in X-ray diffraction (XRD) experiment. Cu *Kα* (λ=0.154 18 nm) was used as radiation. The operating current and voltage were 40 kV and 100 mA, respectively, and the scan range was $10° \leqslant 2\theta \leqslant 80°$. N_2 adsorption-desorption was tested on automatic instrument Quadrasorb SI. The samples were vacuumed at 300 ℃ to eliminate impurity, and then analyzed at −196 ℃ in liquid nitrogen. Renishaw in Via Raman Laser spectrometer was used in Raman spectrum analysis. The wavelength of the excitation was 785 nm and the resolution was 1.5 cm^{-1}. The data collection was carried out at indoor temperature. The scanning scale was 100~2 000 cm^{-1}. X-ray photoelectron spectroscopy (XPS) was operated on an electron spectrometer XSAM-800. Al *Kα* served as source of X-ray. C1*s* (284.8 eV) was used to check the electron binding energy. OSC was tested within a fixed bed reactor. Samples were first heated for 1 h in H_2 at 550 ℃ and then cooled to 200 ℃ in N_2. O_2 was pulse injected into the sample during the test. The signal was detected by thermal conductivity detector (TCD). H_2-temperature - programmed reduction (H_2-TPR) was operated in micro-reactor. The samples were first purged with N_2 at 450 ℃. Then, they were cooled to ambient temperature. In the process of test, the samples were heated to 900 ℃ at the rate of 10 ℃·min^{-1} in mixture gas of H_2/N_2 (5∶95, *V*/*V*).

1.4 Catalytic activity test

A packed bed was used as reactor to test catalytic performance. The measured waste gas was composed of 0.86% CO, 0.06% C_3H_8, 0.12% NO, 12% CO_2 and 10% H_2O (volume fraction). O_2 was adjustable. N_2 was balance gas. The space velocity in reaction was 40 000 h^{-1}. Automotive exhaust analyzer (FGA-4100) was used to detect pollutant concentration.

2 Results and discussion

2.1 XRD and N_2 adsorption-desorption

Fig.1 shows the XRD patterns of CeZr samples. In Fig.1, the major peaks of all samples are characteristic of cubic fluorite structure. The diffraction peak of isolated ZrO_2 couldn't be observed, indicating that CeO_2-ZrO_2 solid solutions are formed. The samples calcined at 500, 600 and 700 ℃ have large and diffuse diffraction peaks, indicating their low crystallinity. With the further raising of temperature, more intensive diffraction peaks could be observed. The result reveals an increase in crystallinity, which is ascribed to agglomeration and sintering of CeO_2-ZrO_2 crystallites. Mean-

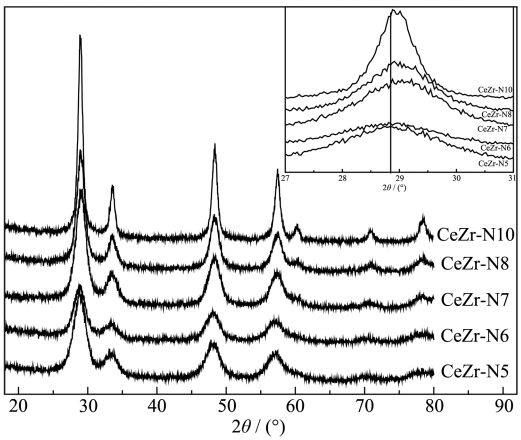

Fig.1　XRD patterns of CeZr

Table 1　Lattice parameters and texture property of CeZr

Sample	Cell parameter / nm	Crystal size / nm	Surface area / ($m^2 \cdot g^{-1}$)	R_{mean} / nm	*V* / ($mL \cdot g^{-1}$)
CeZr-N5	0.531 5	5.2	168	3.0	0.29
CeZr-N6	0.529 9	5.2	144	3.5	0.27
CeZr-N7	0.528 4	5.5	123	4.2	0.26
CeZr-N8	0.528 2	6.6	89	5.9	0.26
CeZr-N10	0.527 1	9.7	61	5.8	0.18
CeZr-A10	0.530 3	10.8	16	15.2	0.1

while, the BET surface area of samples decreased (Table 1). The grain size increased to 9.7 nm and BET surface area decreased to 61 $m^2 \cdot g^{-1}$ after calcination temperature increased to 1 000 ℃. But the growth of grains and decrease of BET surface area were significantly less than CeZr-A10. The results declare that the coexistence of amorphous carbon powder can prevent the particles from growing up very well at low temperature. But when the temperature rises, the role is weakened. It is clarified by the fact that the thermodynamic force is small at low calcination temperature and cannot provoke the growth of Ce-Zr grains. Thus, inhibitory action of carbon powder preponderates. In this case, the resulting Ce-Zr oxides have low crystallinity[9]. When the thermodynamic force becomes powerful and dominant at high calcination temperature, it suppresses the effect of coexisting carbon powder and then Ce-Zr grains grow up.

In order to investigate the shift of the peaks, the diffraction of (111) crystal plane was amplified and listed in the inset of Fig.1. As can be seen when the calcining temperature rose from 500 to 1 000 ℃, the peaks moved to higher diffraction angle and cell parameters dropped from 0.531 5 to 0.527 1 nm owing to the shrinkage of the lattice, which arose from insertion of Zr^{4+} into CeO_2 lattice. The ionic radius of Ce^{4+} is 0.097 nm, which is bigger than Zr^{4+} (0.084 nm)[11-12]. So, the substitution of Zr^{4+} for Ce^{4+} leads to the shrinkage of crystal cell. Much larger shift in peak position is attributed to more insertion of Zr^{4+} ions into the ceria lattice[4]. It is worthwhile to point out that no distinguishable separated phases or asymmetric peaks could be observed, even the calcination temperature high up to 1 000 ℃, which is probably attributed to overlap of the diffraction profiles. As it can be verified by the following discussion of Raman result, the samples calcinated at 800 and 1 000 ℃ had two apparent distinct peaks. However, traditional diffraction analysis cannot differentiate Ce-rich phase from Zr-rich phase when they are coexistence, since their crystalline structure is almost the same[13-14].

As shown in Table 1, it is obviously that raising the calcination temperature leads to decline of the surface area. The decrease of surface area ranks in the order of CeZr-N5>CeZr-N6>CeZr-N7>CeZr-N8>CeZr-N10. The result demonstrates that in the inert atmosphere, collapse of pore structure still can't be avoided at high temperature. The reason is that with the raising of calcination temperature, thermal shrinkage of amorphous carbon gradually becomes aggravated, and its supporting role to pore canal is weakened. And then, collapse of pore structure occurred, which led to decrease of BET surface area. The BET surface area of CeZr-N10 was 61 $m^2 \cdot g^{-1}$, which was more than three times of CeZr-A10. The result indicates that the thermal stability of the sample can be remarkably improved as it is prepared by soft-hard method. The reason is that the destruction of pore structure can be alleviated in a certain degree due to the formation of amorphous carbon in inert atmosphere which can support the pore wall of samples. In order to investigate ultimate thermal stability of CeZr-N10, it was calcined at 1 000 ℃ for another 6 h. After calcined, the BET surface area declined to 28 $m^2 \cdot g^{-1}$, pore diameter increased to 7.2 nm and pore volume decreased to 0.1 $mL \cdot g^{-1}$. The results demonstrate sintering of the sample at high calcination temperature in the absence of amorphous carbon. Though the BET surface area of aged CeZr-N10 declined, it was still higher than CeZr-A10 (16 $m^2 \cdot g^{-1}$), indicating higher thermostability of CeZr-N10. To our knowledge, the BET surface area of aged CeZr-N10 was relatively large compared to other CeO_2-ZrO_2 materials with high content of Ce. That is to say, soft-hard method can improve anti-sintering ability of CeO_2-ZrO_2 materials.

2.2 Raman spectra

Raman spectrum was used to explore existence of carbon and structure of the final materials. A typical spectrum of intermediate products roasting in N_2 at 700 ℃ (CeZr-N7-C) is shown in Fig.2a. As shown in Fig.2a, CeZr-N7-C displayed two bands around 1 600 and 1 350 cm^{-1}, which are attributed to graphite carbon and disordered carbon, respectively[7]. After calcinated in air at 450 ℃, the two bands mentioned above disappeared (Fig.2a, CeZr-N7), indicating the complete removal of carbon. The final samples (Fig.2b) displayed

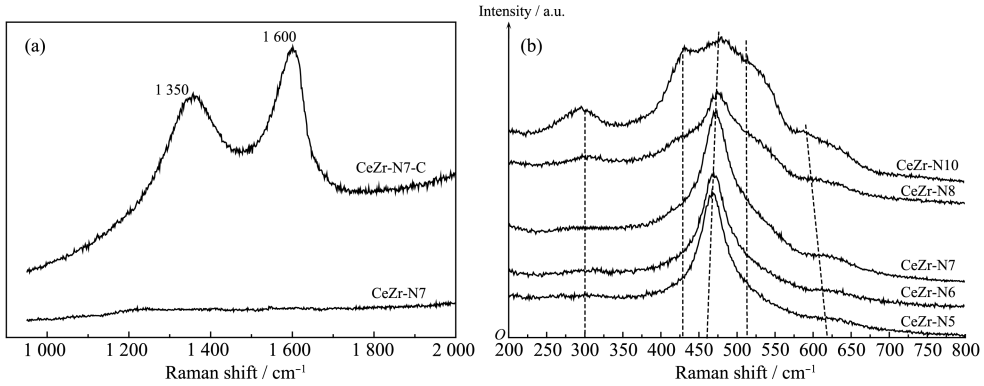

Fig.2　Raman spectra of CeZr

two bands at 462~478 cm^{-1} and 620 cm^{-1}, respectively. The band located at 462~478 cm^{-1} was strong. It is attributed to symmetric vibration of Ce-O bond (F_{2g}) in cubic fluorite CeO_2[15]. No band attributed to ZrO_2 can be observed. The result declares that cerium zirconium solid solution is formed, which agrees with XRD result. With the rise of calcination temperature, the peak at 462 cm^{-1} moved to high band, which demonstrates that more Zr^{4+} insert into ceria lattices at high temperature. As it has been reported that the increase of Zr content in the ceria-zirconia solution can make the vibration of Ce-O bond band shift to higher wave number[16]. The band at 620 cm^{-1} belongs to intrinsic oxygen vacancies in the lattice, which arise from the addition of Zr into the CeO_2[4]. When calcination temperature rose from 500 to 1 000 ℃, the intensity of peak at 620 cm^{-1} increased and shifted to low wavenumber, demonstrating increase of oxygen vacancies. Besides the two bands mentioned above, another two bands at 430 and 515 cm^{-1} could be observed for CeZr-N8 and CeZr-N10, indicating segregation of Zr-rich phase of sample because of calcination at high temperature in inert atmosphere. Nevertheless, owing to its poor diffraction ability of oxygen atoms, XRD cannot distinguish such phase separation from cubic structure. Previous studies have been proposed that phase separation of CeO_2-ZrO_2 oxide may be promoted by surface energy[17-18]. If the grain size is below the critical value, the solid solution is stable. If it exceeds a crucial point, the proportion of surface energy to the total energy of the system is so small that it cannot maintain the stability of crystal, which results in phase separation, and then much stabler Ce-rich and Zr-rich phases are formed. Combined with the XRD result, we deduce that phase segregation of the sample at high temperature may be attributed to increase of crystal size because of sintering. Note also that with elevating of calcination temperature, the peaks at 302 and 620 cm^{-1} became strong, which implies that high calcination temperature at inert atmosphere can create more oxygen vacancies. Two reasons may be account for this. One is that more Ce^{4+} ions are reduced to Ce^{3+} by amorphous carbon at high calcination temperature, which will be confirmed by XPS result. The other possibility is that the segregation of Ce-Zr may induce the formation of Ce-rich and Zr-rich oxides, which is responsible for the increase of structure defect[19].

2.3　XPS spectra

The surface composition and the cerium oxidation state are shown in Table 2 and Fig. 3. Eight peaks could be observed in the Ce3*d* spectra of CeZr (Fig.3). The peaks marked as “v” are characteristic peaks of Ce3$d_{5/2}$, while peaks marked as “u” are characteristic peaks of Ce3$d_{3/2}$. The bands labeled as (v_0, u_0), (v_2, u_2) and (v_3, u_3) are characteristic of Ce^{4+}. Those labeled as (v_1, u_1) are related to Ce^{3+}[20]. It can be seen form Fig.3, the bands labeled as v_1 and u_1 couldn't be distinguished clearly, which indicates that cerium in all the oxides exists mainly in Ce^{4+}. Table 2 summarizes the result of the surface elemental distribution. It is found that the molar ratio of the Ce to Zr (n_{Ce}/n_{Zr}) in all CeZr samples descended with the rise of calcination temperature. The n_{Ce}/n_{Zr} in CeZr-N5 and CeZr-N6 was 2.02 and 1.92, respectively, which exceeded theoretic atom-

Table 2 Surface elemental content of CeZr and Pd/CeZr

Sample	Surface composition / %[a]				n_{Ce}/n_{Zr}	f_{u_3} / %[b]	$x_{Pd^{2+}}$[c]
	Ce3*d*	Zr3*d*	O1*s*	Pd3*d*			
CeZr-N5	17.06	8.68	74.26	—	2.02	16.64	—
CeZr-N6	16.67	8.65	74.68	—	1.92	16.40	—
CeZr-N7	17.49	9.45	73.06	—	1.85	16.39	—
CeZr-N8	16.92	9.72	73.36	—	1.74	16.04	—
CeZr-N10	16.07	9.88	74.05	—	1.63	15.49	—
Pd/CeZr-N5	16.50	8.37	73.93	1.20	1.97	17.25	100%
Pd/CeZr-N6	16.80	8.89	73.04	1.27	1.89	17.04	100%
Pd/CeZr-N7	17.25	9.36	72.10	1.29	1.84	16.88	100%
Pd/CeZr-N8	16.40	9.51	72.94	1.15	1.72	16.39	100%
Pd/CeZr-N10	15.96	9.96	73.02	1.06	1.62	16.13	100%

[a] Molar fraction; [b] Aarea fraction of u_3 peak to all the characteristic peaks of Ce3*d*; [c] Molar fraction, $x_{Pd^{2+}}=n_{Pd^{2+}}/n_{Pd}\times100\%$.

ic ratio, suggesting that the surfaces of CeZr-N5 and CeZr-N6 are richer in Ce than anticipated. It may be because that Zr^{4+} can't be easily intercalated into CeO_2 lattice at relative low calcination temperature. Zhao's[21] study has shown that the insertion of Zr^{4+} into CeO_2 lattice increased gradually with calcination temperature rising, until homogeneous solid solution formed. As it is proved by XRD result, the cell parameters of CeZr-N5 and CeZr-N6 are bigger than the others. Raman spectrum result also demonstrates that the intensity of peak at 620 cm^{-1} associated with oxygen vacancies increased with the rise of calcination temperature. The XRD and Raman spectrum results further testify that the insertion of Zr^{4+} into CeO_2 is progressive. So, Ce-rich phase forms in outer part at relative low temperature. The n_{Ce}/n_{Zr} in CeZr-N7 was 1.85, which was near to the theoretical value (1.86) and indicates that more Zr^{4+} ions insert into ceria lattices and

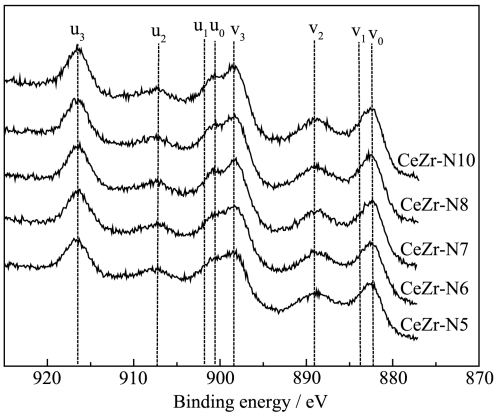

Fig.3 Ce3*d* XPS spectra of CeZr

well element homogeneity of it. However, the n_{Ce}/n_{Zr} in CeZr-N8 and CeZr-N10 were much lower than the theoretic atomic ratio, indicating that the outer parts of the two samples are Zr-rich. Such finding is consistent with the assumption that crystalline phase of CeZr-N8 and CeZr-N10 is a combination of cubic Ce-rich and tetragonal Zr-rich mixed phase, as confirmed in Raman spectrum result. Previous researches[2,4] have revealed that high temperature treatment to CeZr makes Zr^{4+} move from bulk to surface, and at last samples rich in tetragonal Zr phase form at outer space. Our work conforms with the literatures.

The relative molar ratio of Ce^{3+} in the surface region can be assessed indirectly by the fraction of u_3 peak (f_{u_3}). The higher the f_{u_3} is, the lower molar ratio of the Ce^{3+} is. The results are also presented in Table 2. Ce^{3+} content in CeZr samples is found to increase with the calcination temperature. For CeZr-N5, CeZr-N6 and CeZr-N7, the increase of Ce^{3+} with the rise of calcination temperature is attributed to improvement of homogeneity of solid solution. As it was reported in literature[22-23], homogenous CeO_2-ZrO_2 solid solution is in favor of formation of Ce^{3+} or development of oxygen vacancies. Although phase segregation occurs in CeZr-N8 and CeZr-N10, their Ce^{3+} ratio is even higher than CeZr-N7. The high Ce^{3+} ratios of CeZr-N8 and CeZr-N10 are probably attributed to following two reasons: (i) the formation of CeO_2-ZrO_2 nanocrystalline oxides with Ce-rich and Zr-rich domains induces the increase

of structure defect as proved by Raman spectra; (ii) more Ce^{4+} is reduced to Ce^{3+} by amorphous carbon at high calcination temperature. High ratio of Ce^{3+} is favorable to redox property of CeZr, which will be proved by OSC and H_2-TPR results next.

It can be seen from Table 2, after Pd is loaded on the CeZr, the ratio of Ce/Zr and Ce^{3+} decreased slightly. This is attributed to adsorption of Pd species on surface defect sites of CeZr[24-25]. The variation of n_{Ce}/n_{Zr} and Ce^{3+} ratio in Pd/CeZr are in accordance with their corresponding supports. The content of Pd on surface increased in the order of Pd/CeZr-N10<Pd/CeZr-N8<Pd/CeZr-N5<Pd/CeZr-N6<Pd/CeZr-N7. It has been disclosed that the dispersion of Pd species is related to surface area of support and interaction of Pd/CeZr, and large surface area and strong interaction between Pd and CeO_2-ZrO_2 are in favor of dispersion of Pd[26]. For Pd/CeZr-N7, Pd/CeZr-N8 and Pd/CeZr-N10, the dispersion of Pd species is depend on surface area of support. While for Pd/CeZr-N5, Pd/CeZr-N6 and Pd/CeZr-N7, the dispersion of Pd species may be related to interaction between Pd and CeZr support. As shown in Fig.4, Pd3*d* spectra can be fitted into two peaks. The peaks located in a range of 336.9~337.3 eV belong to Pd3$d_{5/2}$, while those located at 341.6~342.3 eV belong to Pd3$d_{3/2}$. These peaks are all attributed to Pd^{2+}. The result indicates that Pd species in all the catalysts exist mainly in the form of Pd^{2+}. The binding energy of Pd3$d_{5/2}$ increases in the sequence of Pd/CeZr-N5<Pd/CeZr-N6<Pd/CeZr-N7. As it has been reported that the increase of binding energy of Pd3$d_{5/2}$ is ascribed to strong interaction between Pd species and support[27]. So, the stronger interaction between Pd and CeZr-N7 imparts Pd/CeZr-N7 higher dispersion of Pd species than those of Pd/CeZr-N6 and Pd/CeZr-N5.

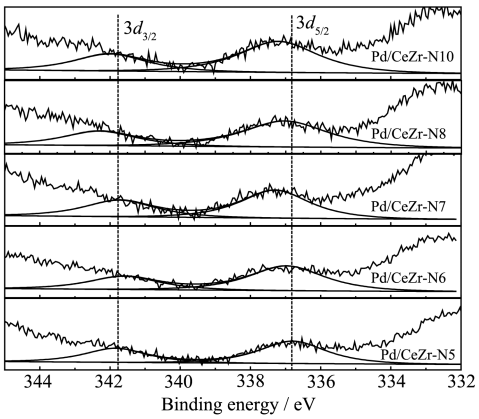

Fig.4　Pd3*d* XPS spectra of Pd/CeZr

2.4　OSC and H_2-TPR

OSC is an important indicator of TWC. It can adjust the balance between reductants and oxidants during purifying automobile exhaust and speed the transfer of oxygen atoms, which is benefit to oxidation reaction at low temperature[28]. The OSC result of CeZr is presented in Fig.5. It can be found from Fig.5 that with elevation of calcination temperature from 500 to 1 000 ℃, the OSC value rose from 730 to 900 μmol·g^{-1}. For CeZr-N5, CeZr-N6 and CeZr-N7, the increase of OSC is due to the improvement of homogeneity of CeO_2-ZrO_2 solid solution. As it was reported, improving the structural homogeneity of CeO_2-ZrO_2 tends to facilitate its OSC and redox capabilities[2]. Although phase separation occurred in CeZr-N8 and CeZr-N10, they had higher OSC value than the others. Two factors may be responsible for this. One is that phase reorganization of Ce and Zr atoms results in lattice distortion at the interfacial atomic layers, which creates more labile oxygen atoms[5]. The other reason is that inhomogeneous phase composition of the sample promotes the formation of interfacial boundaries, which leads to superior oxygen storage capacity[29]. Previous research has shown that the number of oxygen vacancies which is directly in proportion to the concentration of Ce^{3+} is a crucial aspect for OSC of CeO_2-based oxygen storage materials[30]. In our study, the order of OSC value is perfectly consistent with the content of Ce^{3+}.

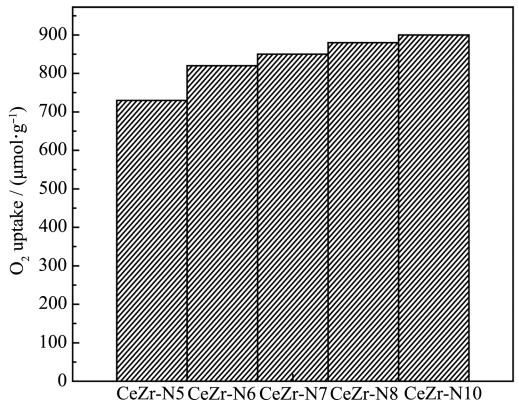

Fig.5　OSC results of CeZr

TPR results of CeZr and their corresponding catalysts are shown in Fig.6 and 7, respectively. Generally, the reduction of CeO_2-ZrO_2 can be divided into two regions at about 500 and 800 ℃. The reduction peak at 500 ℃ is assigned to the behavior of surface oxygen, while the peak at 800 ℃ is ascribe to the behavior of bulk oxygen[31]. However, in the current work, CeZr-N5, CeZr-N6 and CeZr-N7 all showed a broad reduction peak following an asymmetric form in a range of 510~550 ℃, suggesting that the reduction peaks of surface and bulk Ce^{4+} species are overlapped. CeZr-N8 showed a main reduction peak located around 560 ℃ with an obvious shoulder peak around 530 ℃ by the reason of phase separation. While for CeZr-N10, two obviously separated peaks located at 505 and 570 ℃ could be observed owing to more serious phase segregation than CeZr-N8. The two peaks derive from various oxygen species with diverse reducibility which coexist in CeZr-N8 and CeZr-N10. It is attributed to mixed phase composition of CeZr-N8 and CeZr-N10, which is consistent with Raman spectrum and XPS results. The max reduction temperature declines in the sequence of CeZr-N10 >CeZr-N8>CeZr-N5>CeZr-N6>CeZr-N7. The reduction temperature of CeZr-N7 was lowest despite its relatively smaller surface area than CeZr-N6 and CeZr-N5. Thus, it can be concluded that improvement the uniformity of CeO_2-ZrO_2 mixed oxides can prominently modify oxygen environment around Ce and Zr. While for CeZr-N10 and CeZr-N8, they are inclined to be reduced at relatively high temperature owing to their relatively low surface area and heterogeneous phase structure. CuO was used as reference material to estimate H_2 consumption of the samples. The results for CeZr-N5, CeZr-N6, CeZr-N7, CeZr-N8 and CeZr-N10 were 540, 636, 654, 680 and 880 $\mu mol \cdot g^{-1}$, respectively. It is apparent that the H_2 consumption increases when calcination temperature goes up. As it was reported that the depletion of H_2 is strongly associated with the accessible reactive oxygen present in Ce-Zr mixed oxides[19]. Combined with Raman spectrum and XPS results, the increase of H_2 consumption is attributed to phase rearrangement of the sample calcined at high temperature which creates more labile oxygen atoms. The result is also in accordance with Zhang′s[19] study. As for CeZr-A10, it showed a relatively low intensity reduction peak at 570 ℃ and its H_2 consumption was 310 $\mu mol \cdot g^{-1}$. The high reduction temperature and low H_2 consumption of CeZr-A10 demonstrate its poor reducibility due to serious sintering which results in decrease of oxygen vacancies and labile oxygen atoms.

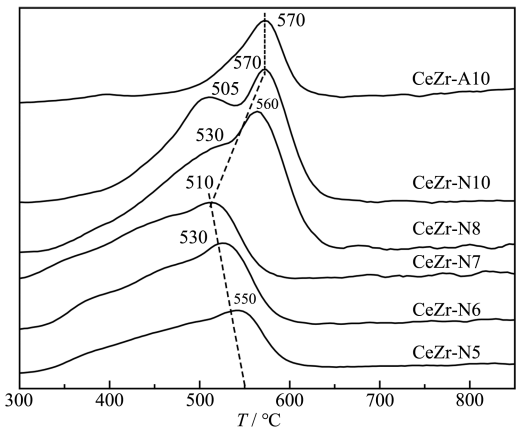

Fig.6 H_2-TPR profiles of CeZr

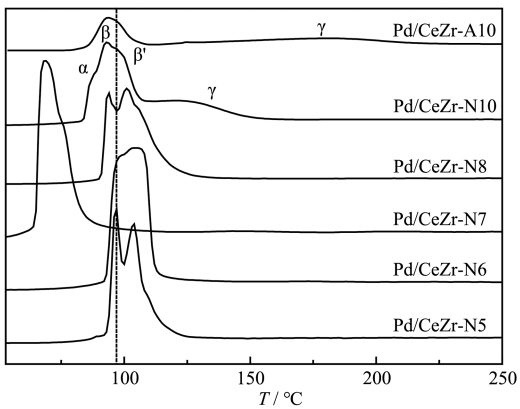

Fig.7 H_2-TPR profiles of the catalysts

The H_2-TPR spectra of Pd/CeZr catalysts are shown in Fig. 7. Unlike the supports, reduction in the catalysts happened at relatively low temperature (below 200 ℃) due to reduction of PdO species. As presented in Fig. 7, calcination temperature of the supports has significant effect on their corresponding Pd only catalysts. Pd/CeZr-N5 showed two hydrogen depletion peaks (denoted as α and β, respectively) in low temperature zone because of its relatively low homogeneous of phase structure. According to previous literature[32], α peak is derived from the reduction of uniform distribution PdO species, while β peak arises from the reduc-

tion of steady PdO species possessing strong mutual effect with supports. Compared with Pd/CeZr-N5, Pd/CeZr-N6 and Pd/CeZr-N7 exhibited unimodal reduction features due to improvement of homogeneity, but the reduction peaks were somewhat asymmetric. It is notable that Pd/CeZr-N8 and Pd/CeZr-N10 catalysts exhibit a splitting of β peak owing to the phase separation of the supports. In addition, another peak γ was observed in Pd/CeZr-N10, which is connected to surface oxygen reduction[33]. The occurrence of γ peak arises from weak mutual effect between the support and PdO, which is in accordance with heterogeneity of Pd/CeZr-N10. As for Pd/CeZr-A10, because of more severe sintering, its reduction temperature of γ peak was higher than Pd/CeZr-N10. The maximum peak temperature for all the catalysts increases as the following order: Pd/CeZr-N7<Pd/CeZr-N8≈Pd/CeZr-N10≈Pd/CeZr-A10<Pd/CeZr-N6≈Pd/CeZr-N5. Hydrogen consumption of Pd/CeZr-N5, Pd/CeZr-N6, Pd/CeZr-N7, Pd/CeZr-N8, Pd/CeZr-N10 and Pd/CeZr-A10 was 710, 925, 928, 625, 523 and 460 $\mu mol \cdot g^{-1}$, respectively, which is far greater than theoretical hydrogen consumption of Pd owing to the strong mutual effect between Pd and CeO_2-ZrO_2 support. It is so-called “spillover effect”[34]. It has been disclosed that hydrogen consumption is related to dispersion of Pd and oxidative Pd^{2+} species, and higher dispersion of Pd and more Pd^{2+} species are conducive to improving hydrogen consumption[35]. Based on XPS result, hydrogen consumption is in consistent with the Pd content in the surface of the catalysts. It is worth noting that high H_2 consumption of the supports may not coincide with high H_2 consumption of their corresponding catalysts. For example, CeZr-N10 had highest H_2 consumption, while Pd/CeZr-N10 possessed lowest H_2 consumption among the catalysts prepared by soft-hard template method. H_2 consumption of CeZr-N7 was significantly lower than CeZr-N10, but Pd/CeZr-N7 possessed highest H_2 consumption, which may be ascribed to high dispersion of Pd on CeZr-N7 and strong interaction between Pd and CeZr-N7 as proved by XPS result. Highly dispersed Pd and strong interaction between Pd and the supports are benefit to more available reducible species including PdO species and some Ce^{4+} species promoted by Pd[36]. So, reducibility of the support and the catalyst is not highly correlated. It was also disclosed in Li′s[37] study that H_2 consumption of fresh Pd/CZAc was higher than Pd/CZAm, while H_2 consumption of their supports was inverse. Pd/CeZr-N7 possessed lowest reduction temperature and highest H_2 depletion, indicating the best redox capability of it. It may be attributed to uniform distribution of Pd on CeZr-N7 on account of strong mutual effect between Pd and CeZr-N7. Though the reduction temperature of Pd/CeZr-N6 was slightly higher than Pd/CeZr-N8 and Pd/CeZr-N10, its H_2 consumption was almost equal to Pd/CeZr-N7. In this regard, Pd/CeZr-N6 also behaves excellent redox property. Comprehensive consideration reduction temperature and total H_2 depletion, the redox performance rises in the sequence of Pd/CeZr-A10<Pd/CeZr-N10<Pd/CeZr-N8<Pd/CeZr-N5<Pd/CeZr-N6<Pd/CeZr-N7. Among all the catalysts prepared by soft-hard template method, Pd/CeZr-N10 behaves the worst reduction performance because of the sintering of the support at high calcination temperature, but its reduction performance is significantly better than Pd/CeZr-A10. So, it can be concluded that soft-hard template method imparts catalyst better thermal stability.

2.5 Three-way catalytic performance

The conversions of C_3H_6, CO and NO over Pd/CeZr are showed in Fig. 8. Table 3 also provides T_{50} (light-off temperature) and T_{90} (full-conversion temperature) of C_3H_8, CO and NO. In comparison, the activity of Pd/CeZr-A10 is also showed in Fig. 8 and Table 3. Based on the data in Fig. 8 and Table 3, T_{50} and T_{90} of C_3H_8, CO, NO on Pd/CeZr-N7 were lowest, demonstrating its excellent catalytic activity. T_{50} and T_{90} of C_3H_8, CO, NO on Pd/CeZr-N6 were slightly higher than on Pd/CeZr-N7, but significantly lower than on other catalysts, indicating its lower activity than Pd/CeZr-N7 but higher activity than others. The T_{50} of CO over Pd/CeZr-N5 and Pd/CeZr-N8 were the same, but conversion of C_3H_8 and NO over Pd/CeZr-N5 were about 10 ℃ lower than those on Pd/CeZr-N8. The result indicates that Pd/CeZr-N5 exhibits better activity for conversion of C_3H_8 and NO than Pd/CeZr-N8. The T_{50} of C_3H_6, NO and CO over Pd/CeZr-N8 were 262, 163 and 120 ℃, respectively,

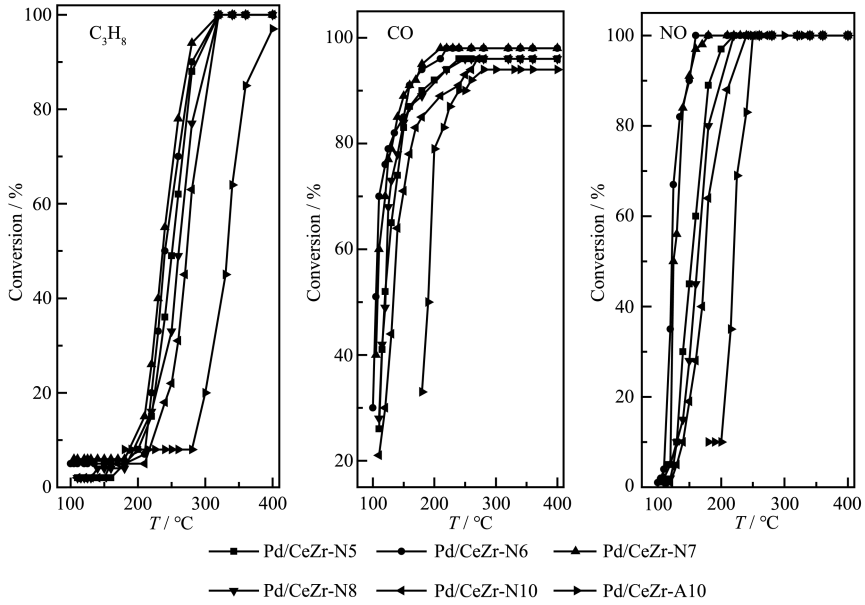

Fig.8 Conversion of C_3H_8, CO and NO over Pd/CeZr at different temperatures

Table 3 T_{50} and T_{90} of C_3H_8, NO, CO on the catalysts

Catalyst	T_{50} / ℃			T_{90} / ℃		
	C_3H_8	NO	CO	C_3H_8	NO	CO
Pd/CeZr-N5	251	152	120	290	185	180
Pd/CeZr-N6	240	125	105	285	150	152
Pd/CeZr-N7	238	120	108	280	150	150
Pd/CeZr-N8	262	163	120	300	200	185
Pd/CeZr-N10	274	175	133	310	216	201
Pd/CeZr-A10	335	220	190	365	245	225

which is clearly lower than those of Pd/CeZr-N10, suggesting that Pd/CeZr - N8 possesses better catalytic property than Pd/CeZr - N10. The T_{50} and T_{90} of C_3H_6, NO, CO over Pd/CeZr - A10 were significantly higher than Pd/CeZr-N10, which indicates the activity of Pd/CeZr-A10 is worse than Pd/CeZr - N10. Based on the above analysis, the activity of the catalysts declines in sequence of Pd/CeZr - N7>Pd/CeZr - N6>Pd/CeZr - N5>Pd/CeZr - N8>Pd/CeZr - N10>Pd/CeZr - A10. Following two reasons may be account for the result: (i) Pd/CeZr-N7 shows best dispersity of Pd species than other catalysts. Highly dispersed Pd can offer more active sites which are benefit to catalytic reaction. As disclosed by XPS result, the content of Pd species follows a decline of Pd/CeZr-N7>Pd/CeZr-N6>Pd/CeZr-N5>Pd/CeZr-N8>Pd/CeZr - N10, which agrees with the activity of the catalysts. (ii) The excellent reducibility of the highly dispersed PdO_x species is benefit to the activity of the catalysts. As it has been reported that excellent reduction performance is benefit to oxidation of CO and C_3H_8[38-39]. In addition, outstanding reducibility is also in favor of the reaction between adsorbed oxygen and reductant, hence the improvement of reduction to NO[40]. It can be seen in our study the activity is consistent with the reducibility of the catalysts. Despite extraordinary OSC performance of CeZr-N10, its corresponding catalyst Pd/CeZr-N10 showed the worst three-way activity among the catalysts prepared by the same method. It is possible. As it has been found in Muraki's study that $Rh/CeO_2 - ZrO_2$ with higher OSC presented lower activity than Rh/CeO_2 with lower OSC[41]. Kusatsugu's study[42] also disclosed negative effect of OSC on activity of Fe - doped $Pd/CeO_2 - ZrO_2$ when the OSC was too high. Kolli[43] discovered that Pd/Al_2O_3-$Ce_{0.75}Zr_{0.25}O_2$-La_2O_3 with high dynamic OSC showed low CO oxidation efficiency because of smaller

surface area than $Pd/Ce_{0.75}Zr_{0.25}O_2$-Al_2O_3. So, low activity of Pd/CeZr-N10 may be attributed to the decline of Pd dispersity and reduction capacity induced by its low BET surface area. As proved by XPS and H_2-TPR results, Pd/CeZr-N10 possessed lowest surface Pd content and worst redox performance. As for Pd/CeZr-N5, Pd/CeZr-N6 and Pd/CeZr-N7, the activity is in accordance with OSC and reduction capacity. The result proves the importance of Pd dispersion and reducibility to catalytic performance once again. T_{50} and T_{90} for C_3H_8, NO and CO of unit specific surface on catalysts are listed in Table 4. It is obviously that the specific activity is connected to specific area of catalyst. Combined with the BET surface area, the specific activity increased with the rising of surface area. As large surface area is benefit to dispersity of PdO and provides more approachable active sites, the catalytic activity is improved[44]. Though Pd/CeZr-A10 and Pd/CeZr-N10 were calcined at the same temperature, Pd/CeZr-A10 possessed worse activity than Pd/CeZr-N10 because of severe sintering. The result indicates that the catalysts prepared by soft-hard template method have excellent thermal stability.

Based on above analysis, conclusions can be drawn as follows: (i) the calcination temperature of the supports has outstanding effect on the catalytic performance of their corresponding catalysts; (ii) the dispersity of Pd and reduction property of the catalysts are key factors affecting the catalytic performance; (iii) the specific activity is positive correlation to the specific area of the catalyst; (iv) soft-hard template method can impart the excellent thermal stability of the catalysts.

Table 4　T_{50} and T_{90} of C_3H_8, NO, CO on unit specific surface of the catalysts

Catalyst	T_{50} / (℃·g·m^{-2})			T_{90} / (℃·g·m^{-2})		
	C_3H_8	NO	CO	C_3H_8	NO	CO
Pd/CeZr-N5	1.49	0.9	0.71	1.73	1.10	1.07
Pd/CeZr-N6	1.67	0.87	0.73	1.98	1.04	1.06
Pd/CeZr-N7	1.93	0.98	0.88	2.28	1.22	1.22
Pd/CeZr-N8	2.94	1.83	1.35	3.37	2.25	2.08
Pd/CeZr-N10	4.49	2.87	2.18	5.08	3.54	3.30
Pd/CeZr-A10	20.94	13.75	11.88	22.81	15.31	14.00

3 Conclusions

In soft-hard template method, calcination temperature has strong effect on structure performance, redox property and activity of $Ce_{0.65}Zr_{0.35}O_2$ supports and their corresponding catalysts. With calcination temperature increasing, the structure properties decline, but the OSC and reduction property of $Ce_{0.65}Zr_{0.35}O_2$ increase because of phase reorganization to form two different phase components with Ce-rich and Zr-rich domains, which result in lattice distortion at the interfacial atomic layers. The redox property of their corresponding catalysts decreases with going up of calcination temperature because of the sintering of the supports which results in decline of three-way catalytic activity. Although high temperature roasting leads to decline of catalytic performance, the catalysts loaded on $Ce_{0.65}Zr_{0.35}O_2$ prepared by soft-hard template method behave excellent activity compared with that calcined direct in air.

References:

[1] Lan L, Chen S H, Li H M, et al. *Mater. Des.*, **2018**,**147**:191-199

[2] Deng J, Yuan S D, Xiong L, et al. *Mater. Charact.*, **2019**,**155**:109808

[3] Cai W, Zhong Q, Zhang S L, et al. *Chem. Eng. J.*, **2014**,**236**:223-232

[4] Zhao B, Li G F, Ge C H, et al. *Appl. Catal. B*, **2010**,**96**:338-349

[5] Lan L, Chen S H, Zhao M, et al. *J. Mol. Catal. A*, **2014**,**394**(15):10-21

[6] Wang Q Y, Zhao B, Li G F, et al. *Environ. Sci. Technol.*, **2010**,**44**(10):3870-3875

[7] Lee J, Oriall M C, Warren S C, et al. *Nat. Mater.*, **2008**,**7**(3):222-228

[8] Xie G Q, Lu J Q, Zheng H Y, et al. *J. Alloys Compd.*, **2010**, **493**(1/2):169-174

[9] Zhang D. *Korean J. Chem. Eng.*, **2008**,**25**(5):1205-1207

[10]HUANG Li-Hua(黄利华), CHEN Shan-Hu(陈山虎), GONG Mao-Chu(龚茂初), et al. *Chinese J. Inorg. Chem.*(无机化学学报), **2016**,**32**(2):193-201

[11]Saada R, Kellici S, Heil T, et al. *Appl. Catal. B*, **2015**,**168**: 353-362

[12]Alla S K, Kollu P, Singh S, et al. *Mater. Res. Bull.*, **2018**,**104**: 65-71

[13]Mamontov E, Brezny R, Manoj M, et al. *J. Phys. Chem. B*, **2003**,**107**:13007-13014

[14]Specchia S, Finocchio E, Busca G, et al. *J. Catal.*, **2009**,**263**: 134-145

[15]Deng J, Li S S, Xiong L, et al. *Mater. Chem. Phys.*, **2019**,**236**: 121767

[16]Reddy B M, Khan A, Yamada Y, et al. *Langmuir*, **2003**,**19**: 3025-3030

[17]Bozo C, Gaillard F, Guilhaume N. *Appl. Catal. A*, **2001**,**220** (1/2):69-77

[18]Kenevey K, Valdivieso F, Soustelle M, et al. *Appl. Catal. B*, **2001**,**29**(2):93-101

[19]Zhang H L, Hu W, Zhou C X, et al. *Appl. Catal. A*, **2018**,**563**: 204-215

[20]Deng J, Li S S, Xiong L, et al. *Appl. Surf. Sci.*, **2020**,**505**: 144301

[21]ZHAO Min(赵明), YU Quan-Wei(余全伟), CAI Li(蔡黎), et al. *Journal of Functional Materials*(功能材料), **2008**(5): 793-796

[22]Gong P J, Xie J L, Fang D, et al. *Chem. Eng. J.*, **2019**,**356**: 598-608

[23]Li S S, He J S, Dan Y, et al. *Mater. Chem. Phys.*, **2020**,**240**: 122150

[24]Deng J, Zhou Y, Li S S, et al. *J. Ind. Eng. Chem.*, **2018**,**64**: 219-229

[25]Hinokuma S, Fujii H, Okamoto M, et al. *Chem. Mater.*, **2010**, **22**:6183-6190

[26]Sekizawa K, Widjaja H, Maeda S, et al. *Appl. Catal. A*, **2000**, **200**(1/2):211-217

[27]Kobayashi T Y T, Kayano T, Kayano K. *Appl. Catal. B*, **2001**, **3**:287-292

[28]Guo J X, Shi Z H, Wu D D, et al. *Mater. Res. Bull.*, **2013**,**48**: 495-503

[29]Lan L, Chen S H, Cao Y, et al. *J. Colloid Interface Sci.*, **2015**, **450**:414-416

[30]Kullgren J, Hermansson K, Broqvist P. *J. Phys. Chem. Lett.*, **2013**,**4**:604-608

[31]Martínez L M, Araque M, Centeno M A, et al. *Catal. Today*, **2015**,**242**(5):80-90

[32]Lin S Y, Yang L Y, Yang X, et al. *Appl. Surf. Sci.*, **2014**,**305**: 642-649

[33]Wang Q Y, Li G F, Zhao B, et al. *Appl. Catal. B*, **2010**,**101**(1/2):150-159

[34]Christou S Y, Costa C N, Efstathiou A M. *Top. Catal.*, **2004**, **30**:325-331

[35]Wu Z L, Li M J, Overbury S H. *J. Catal.*, **2012**,**285**:61-73

[36]Lan L, Yan C Y, Chen S H, et al. *J. Taiwan Inst. Chem. Eng.*, **2018**,**85**:98-105

[37]Li S S, Zhang H L, Dan Y, et al. *J. Mol. Catal.*, **2020**,**482**: 110696

[38]Iglesias-Juez A, Martinez-Arias A, Fernandez-Garcia M. *J. Catal.*, **2004**,**221**:148-161

[30]Hungria A B, Fernandez-Garcia M, Anderson J A, et al. *J. Catal.*, **2005**,**235**:262-271

[40]Barrera A, Viniegra M, Bosch P, et al. *Appl. Catal. B*, **2001**, **34**:97-111

[41]Muraki H, Zhang G. *Catal. Today*, **2000**,**63**:337-345

[42]Kusatsugu K, Nakamura Y, Haneda M. *Appl. Catal. A*, **2019**, **587**:117268

[43]Kolli T, Kroger V, Keiski R L. *Top. Catal.*, **2007**,**45**:165-168

[44]Li S S, Deng J, Dan Y, et al. *Appl. Surf. Sci.*, **2020**,**506**: 144866